arXiv:2505.10641v1 [cs.LG] 15 May 2025

FRET: Feature Redundancy Elimination for Test Time Adaptation

Linjing You[1,*] Jiabao Lu[1,*] Xiayuan Huang[2,†] Xiangli Nie[1]
[1]Institute of Automation, Chinese Academy of Sciences, Beijing, China
[2]College of Science, Beijing Forestry University, Beijing, China
{youlinjing2023, lujiabao2025, xiangli.nie}@ia.ac.cn
huangxiayuan@bjfu.edu.cn

Abstract

Test-Time Adaptation (TTA) aims to enhance the generalization of deep learning models when faced with test data that exhibits distribution shifts from the training data. In this context, only a pre-trained model and unlabeled test data are available, making it particularly relevant for privacy-sensitive applications. In practice, we observe that feature redundancy in embeddings tends to increase as domain shifts intensify in TTA. However, existing TTA methods often overlook this redundancy, which can hinder the model's adaptability to new data. To address this issue, we introduce ***F****eature* ***R****edundancy* ***E****limination for* ***T****est-time Adaptation (****FRET****), a novel perspective for TTA. A straightforward approach (S-FRET) is to directly minimize the feature redundancy score as an optimization objective to improve adaptation. Despite its simplicity and effectiveness, S-FRET struggles with label shifts, limiting its robustness in real-world scenarios. To mitigate this limitation, we further propose Graph-based FRET (G-FRET), which integrates a Graph Convolutional Network (GCN) with contrastive learning. This design not only reduces feature redundancy but also enhances feature discriminability in both the representation and prediction layers. Extensive experiments across multiple model architectures, tasks, and datasets demonstrate the effectiveness of S-FRET and show that G-FRET achieves state-of-the-art performance. Further analysis reveals that G-FRET enables the model to extract non-redundant and highly discriminative features during inference, thereby facilitating more robust test-time adaptation. The code is available at https://anonymous.4open.science/r/fret-21BD.*

1. Introduction

Recently, the emergence of deep neural networks (DNNs) [12, 18] has significantly propelled the advancement in a vast range of human tasks [1, 15, 37]. However, the basic assumption that training and test data are drawn independently and identically (i.i.d.) may not be suitable in many real-world scenarios where the test/target distribution diverges from the training/source distribution [49]. This phenomenon, known as distribution shift, often leads to poor performance [8]. To tackle this issue, a variety of generalization or adaptation techniques have been developed to improve model robustness against distribution shifts [24, 53, 58]. Among these, Test Time Adaptation (TTA) [10, 39, 40] has been the focus of recent and active research. TTA has the advantage of only requiring access to the pre-trained model from the training/source domain and unlabeled test data. Therefore, TTA is a more secure and practical solution especially when models are publicly available but the training data and training process remain

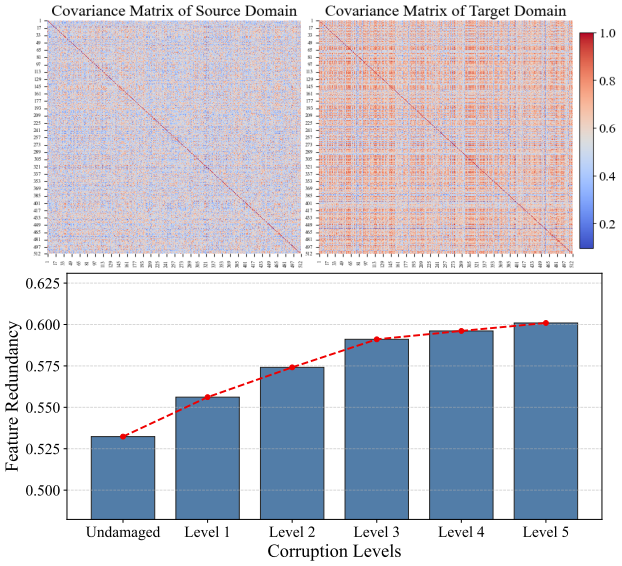

Figure 1. An intuitive demonstration of the relationship between embedded feature redundancy and distribution migration.**Top:** Second-order feature relation graph of embedding features. **Bottom:** Plot of feature redundancy versus the level of corruption.

inaccessible due to privacy and resource restrictions [24].

Existing TTA methods can be broadly categorized into batch normalization calibration methods, pseudo-labeling methods, consistency training methods, and clustering-based training methods, based on different adaptation strategies [24]. Batch normalization (BN) calibration methods [52] posit that the statistics in the BN layers represent domain-specific knowledge. To bridge the domain gap, it is suggested to replace the training BN statistics with new statistics estimated over the entire target domain. Pseudo-labeling methods [57] employ various filtering strategies, such as thresholding or entropy-based approaches, to obtain reliable pseudo-labels. This process helps minimize discrepancies between predicted labels and pseudo-labels. Consistency training methods [38] aim to improve the stability of network predictions or features by addressing variations in input data, such as noise or perturbations, and changes in model parameters. Clustering-based training methods [19] focus on reducing uncertainty in target network predictions by leveraging clustering techniques to organize target features into distinct groups, thereby enhancing the robustness of the model.

Despite the empirical effectiveness of these methods, none of them addresses the issue of feature redundancy in embeddings, which can impair the model's ability to generalize to new data [22]. As depicted in Fig. 1, the feature redundancy in ResNet-18's [12] embeddings on the CIFAR10-C dataset [13] during distribution shifts is illustrated by using a second-order feature relations graph (i.e., covariance matrix of features) [25]. Specifically, ResNet-18 transforms each image into a low-dimensional embedding with 512 features. n embeddings are stacked into an $n \times 512$ matrix, and the absolute values of its covariance matrix (512×512) are computed for visualization. In the resulting heatmap, deeper red colors indicate higher correlation between the corresponding features. Overall, a redder hue suggests higher redundancy within the feature set. The top two images in Fig. 1 shows the second-order feature relation graphs for the source and target domains. Visual inspection reveals that feature redundancy is significantly higher in the target domain compared to the source domain, which highlights the impact of distribution shift on feature redundancy. To further illustrate the relationship between feature redundancy and distribution shift, we remove the diagonal elements of the covariance matrix and calculate the sum of the absolute values of the remaining elements to derive the redundancy scores (see Eq. (1)). As depicted in the bottom of Fig. 1, feature redundancy increases with the level of corruption (i.e., the degree of distribution shift). This suggests that **features with lower redundancy may be better suited for adaptation to the target domain**.

Building on the limitations identified in the existing literature and the observations above, we provide a novel perspective for test-time adaptation—Feature Redundancy Elimination for TTA (**FRET**)—which differs from existing methods. Due to the inherently differentiable nature of the redundancy metric, a straightforward and computationally efficient approach is to directly minimize the feature redundancy score. We refer to this simple approach as S-FRET. However, since S-FRET lacks the ability to perceive label distributions, it effectively addresses **covariate shift** but fails to handle **label shift**—a scenario where the target domain exhibits a label distribution that deviates from the source domain (e.g., long-tailed data). This discrepancy can significantly degrade model performance and remains a critical challenge [3, 16, 31].

To overcome S-FRET's limitation in handling label shift, we further propose G-FRET, which integrates a Graph Convolutional Network (GCN). Unlike FRET, which only minimizes redundancy at the representation layer, G-FRET leverages GCN to incorporate both attention and redundant feature relationships into the representation and prediction layers. Specifically, G-FRET learns non-redundant and discriminative representation through contrastive distillation between attention and redundant representation in the representation-layer. In the prediction layer, attention predictions are optimized through entropy minimization, while ensuring that they are distinct from redundant predictions by negative learning. By maximizing the discriminability of attention relationships while eliminating redundancy in both the representation and prediction layers, G-FRET effectively reduces test-time feature redundancy and improves discrimination when handling complex distribution-shifted test data.

We summarize the contributions of this paper as follows.

- **Potential Way:** provide a novel perspective for test-time adaptation — Feature Redundancy Elimination for TTA (**FRET**) — which differs from existing methods. It adapts the model to distribution shifts by reducing the redundancy of embedded features during testing. To the best of our knowledge, this is the first attempt to leverage feature redundancy for TTA.
- **Innovative Methods:** We propose two novel methods, S-FRET and G-FRET, to eliminate feature redundancy in test-time embeddings. S-FRET directly minimizes the feature redundancy score, offering a lightweight solution. G-FRET extends this by decomposing feature relations into attention and redundancy components, enabling joint optimization of redundancy elimination and class discriminability in real-world scenarios.
- **Extensive Evaluation:** Comprehensive experiments across multiple model architectures, tasks, and datasets demonstrate the effectiveness of S-FRET and show that G-FRET achieves state-of-the-art performance. Further in-depth analysis reveals that G-FRET facilitates the extraction of non-redundant and discriminative embedding

features during testing, ultimately enhancing model adaptation to the test-time target domain.

2. Preliminary and Notations

We briefly revisit Test-Time Adaptation and Feature Redundancy Elimination in this section for the convenience of introducing methods, and put detailed related work discussions into Sec. 6 due to page limits.

2.1. Test-Time Adaptation

In the test-time adaptation (TTA) scenario, we have access only to unlabeled data from the target domain in an online manner and a pre-trained model from the source domain. Specifically, let $\{(x_i, y_i)\}_{i=1}^{n_s} \subset \mathcal{X}_s \times \mathcal{Y}_s$ represent the labeled source domain dataset with labels $\mathcal{Y}_s$ and $\{x_j\}_{j=1}^{n_t} \subset \mathcal{X}_t$ represent a batch of unlabeled target data. The model, trained on the source domain dataset and parameterized by θ, is denoted as $g_\theta = h(f(\cdot)) : \mathcal{X}_s \to \mathcal{Y}_s$, where f is the backbone encoder and h denotes the linear classification head. Our objective is to adapt this model to the target domain $\mathcal{X}_t$, which exhibits a different distribution from that of the source domain $\mathcal{X}_s$. During testing, for each instance $x_j \in \mathcal{X}_t$, let the output of f and h be denoted as embedding $z_j = f(x_j) \in \mathbb{R}^d$ and logits $p_j = h(z_j) \in \mathbb{R}^C$, respectively, where d is the dimension of the embeddings and C is the number of classes.

2.2. Feature Redundancy Elimination

Feature redundancy is a key concern in both feature extraction and feature selection [26, 42]. Following previous work [56], we remove the diagonal elements of the covariance matrix and calculate the sum of the absolute values of the remaining elements to derive the redundancy scores R_e as:

$$R_e = \left\| \tilde{Z}^T \tilde{Z} - I_d \right\|_1 \tag{1}$$

where I_d is the identity matrix, $\|\cdot\|_1$ denotes the 1-norm of a matrix and $\tilde{Z}_{:,j} = \frac{Z_{:,j}}{\|Z_{:,j}\|_2}$ denotes the matrix obtained by normalizing each column.

3. The Proposed Approach

3.1. S-FRET

To eliminate feature redundancy in the target domain, a simple yet effective approach is to directly minimize the feature redundancy R_e, as defined in Eq. (1), leading to the proposed method S-FRET (Simple and Straightforward FRET). The loss function for S-FRET can be written as:

$$\mathcal{L}_{SFRET} = \left\| \tilde{Z}^T \tilde{Z} - I_d \right\|_1 \tag{2}$$

This method directly minimizes the redundancy score derived from feature correlation, providing a computationally efficient solution that avoids complex architectural modifications. By focusing on the feature space of representation-layer, S-FRET enables the model to extract non-redundant representations, thereby enhancing its adaptability to the target domain (see Fig. 3).

However, since the redundancy score does not incorporate information about class distributions, S-FRET primarily addresses **covariate shift** but lacks the discriminative capability to handle **label shift**—a critical challenge where the target domain exhibits a label distribution that deviates significantly from the source domain (e.g., long-tailed data), leading to substantial performance degradation (see Tab. 4) [3, 16, 31].

3.2. G-FRET

3.2.1. Overview of G-FRET

To eliminate feature redundancy and address label shift in the target domain, we further propose a novel two-layer TTA method, namely Graph Convolutional Network based Feature Redundancy Elimination for Test Time Adaptation (G-FRET), which leverages GCN to simultaneously model feature relationships and sample-specific discriminative information in both representation and prediction layers. Fig. 2 provides an overview of our G-FRET framework.

The key idea of G-FRET is to adapt the pre-tarined model during testing by extracting discriminative and non-redundant embedding features from both the representation and prediction layers. Firstly (Sec. 3.2.2), we apply a mask matrix to the second-order feature relation graph. This process yields two separate graphs: an attention graph, which highlights significant feature relationships, and a redundant graph, which identifies redundant feature relationships. Next, we derive the attention/redundancy representation and attention/redundancy prediction by utilizing a single-layer GCN to integrate the model's embeddings with the attention and redundant graphs. This process allows us to explicitly separate attention and redundancy relations in both representation and prediction layer. Then (Sec. 3.2.3), in the representation layer, contrastive learning techniques are employed to enhance the discriminability of the attention representation while ensuring it remains distant from the redundant representation. At last (Sec. 3.2.4), in the prediction layer, attention predictions are optimized through entropy minimization, while ensuring that they are distinct from redundant predictions by negative learning. Through this two-layer process, we achieve discriminative and non-redundant embedding features that effectively adapt to the target domain.

3.2.2. Attention Part and Redundancy Part

Given a batch of n_t data instances from the target domain, we obtain the first-order $n_t \times d$ embedding feature matrix $Z \in \mathbb{R}^{n_t \times d}$ and the second-order feature relation graph

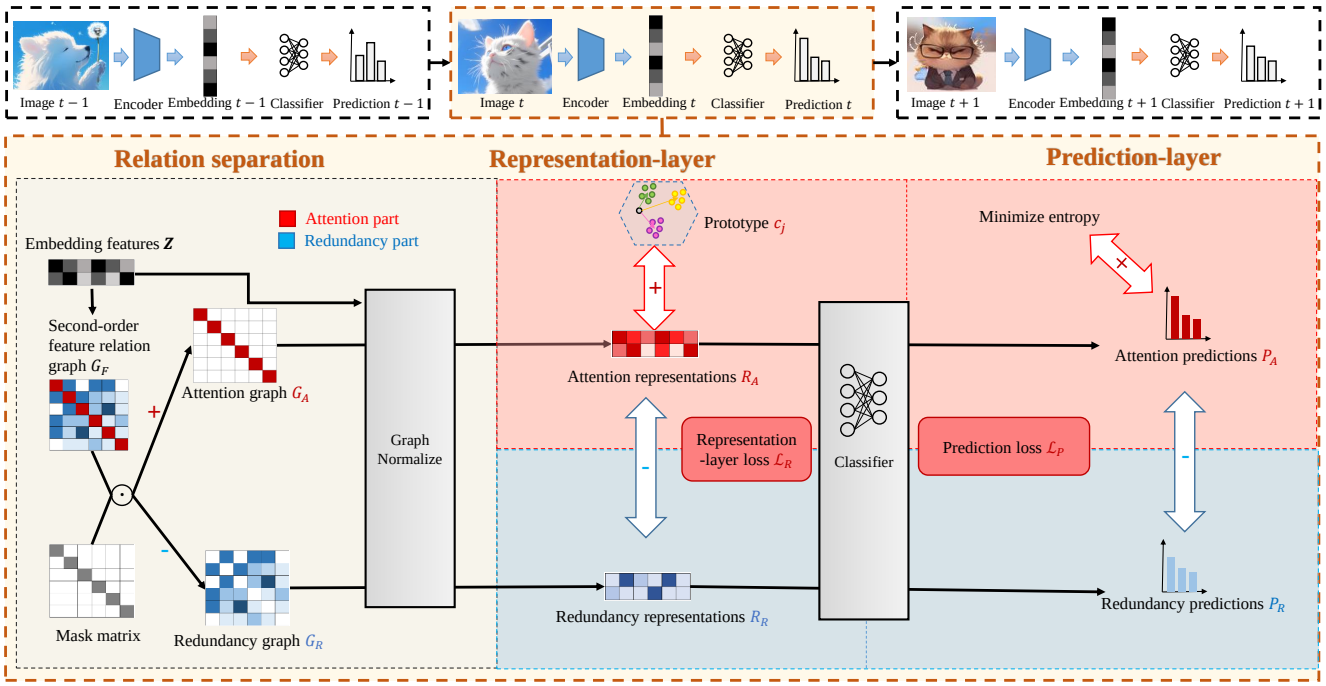

Figure 2. The pipeline of our proposed Graph Convolutional Network based Feature Redundancy Elimination for Test Time Adaptation (G-FRET) method. For each test sample, G-FRET learns non-redundant and discriminative representation through contrastive distillation in the representation-layer. Additionally, in the prediction layer, attention predictions are optimized through entropy minimization, while ensuring that they are distinct from redundant predictions by using negative learning.

$G_F = Z^T Z \in \mathbb{R}^{d\times d}$. Following the state-of-the-art feature selection method SOFT [56], we apply a symmetric mask matrix $M_M \in \mathbb{R}^{d\times d}$ to G_F. This decomposition of G_F yields two distinct graphs: the attention graph G_A and the redundancy graph G_R. G_A captures the attention relations (i.e., important relation) among features, while G_R represents the redundant relation between them. Formally, they are calculated as follows:

$$G_A = G_F \odot M_M; G_R = G_F - G_A \tag{3}$$

where $\odot$ is the element-wise product. However, differently from SOFT, which focuses on feature selection by deriving an optimal mask matrix M_M, our objective is to extract non-redundant features Z. For ideally non-redundant features, the second-order feature relation graph should be a diagonal matrix, indicating that each feature is independent of all others. Therefore, we set $M_M = I_d$ to ensure that G_A captures only the essential feature relations, while G_R includes all remaining relations as redundant relations. Here, $I_d \in \mathbb{R}^{d\times d}$ is the identity matrix. In addition, in some scenarios with prior knowledge, such as knowing which features may be more important, or needing to maintain special structural relations between features, some adaptations can be made by simply modifying the mask matrix M_M.

Then, in order to obtain attention/redundancy representation and attention/redundancy prediction based on the attention and redundancy graphs, we combine the normalized graph matrix with the classifier head h to form a one-layer Graph Convolutional Network (GCN [17]), which can help generate attention representations R_A and attention predictions P_A that contain both data information and feature relationship information:

$$R_A = ZD_A^{-1/2} G_A D_A^{-1/2}; P_A = R_A \theta^h \tag{4}$$

where $D_A^{-1/2} G_A D_A^{-1/2}$ is the normalized graph matrix of graph G_A, D_A is the degree matrix of the graph, and θ^h are the parameters of the classifier head h. Similarly, we can obtain redundancy representations R_R and predictions P_R from redundancy graph G_R:

$$R_R = ZD_R^{-1/2} G_R D_R^{-1/2}; P_R = R_R \theta^h \tag{5}$$

Therefore, we decompose the model's original presentation and prediction into two components: the attention part and the redundancy part. This decomposition enables a distinct focus on important relationships while identifying redundant ones. Specifically, R_A and P_A focus solely on the feature relationships within the attention part, while R_R and P_R are concerned exclusively with the feature relationships within the redundancy part. Based on this decomposition, our goal is to ensure that the attention part adapts effectively to the target domain. Simultaneously, we aim to separate

redundancy part from the attention component in both the representation and prediction layers.

3.2.3. Representation-Layer Redundancy Elimination

With the above representations R_A and R_R, we expect that the attention representations possess class discriminability to handle label shift, while remaining distinct from redundancy representations to eliminate feature redundancy. To achieve this, we leverage contrastive learning [23, 30] as follows:

$$\mathcal{L}_R = -\sum_{i=1}^{n_t} \log \frac{\exp(\text{sim}(R_{A_i}, c_o))}{\sum_{j=1}^{C} \exp(\text{sim}(R_{A_i}, c_j)) + \exp(\text{sim}(R_{A_i}, R_{R_i}))} \tag{6}$$

where $\text{sim}(\cdot,\cdot)$ denotes cosine similarity, $\{c_j\}_{j=1}^{C}$ denote the class centers in the attention representation space, C is the number of clusters, and c_o represents the center of the cluster that contains R_{A_i}. c_j is calculated as follows:

$$c_j = \frac{\sum_i z_i \cdot \mathbf{1}[\text{argmax}(p_i) = j]}{\sum_i \mathbf{1}[\text{argmax}(p_i) = j]} \tag{7}$$

where $\mathbf{1}(\cdot)$ is an indicator function, outputting value 1 if the argument is true or 0 otherwise.

By minimizing $\mathcal{L}_R$, the model simultaneously enhances the discriminability of attention representations while ensuring their distinction from redundancy representations. This process enables the model to extract robust, discriminative, and non-redundant embedding features in the representation layer, facilitating effective adaptation to the target domain.

3.2.4. Prediction-Layer Redundancy Elimination

In the prediction layer, to enhance the discriminability of attention predictions while reducing the influence of redundant predictions, we combine the principles of entropy minimization and negative learning into a unified loss function:

$$\mathcal{L}_P = -\sum_{i=1}^{N} \sigma(P_{A_i}) \log \sigma(P_{A_i}) - \sum_{i=1}^{N} \sigma(P_{R_i}) \log \sigma(1 - P_{A_i}) \tag{8}$$

where σ denotes the softmax operation. Here, the first term minimizes the entropy of attention predictions P_A, encouraging sharper and more confident predictions, while the second term applies negative learning to redundant predictions P_R, penalizing them to ensure they remain distinct from the attention predictions.

3.2.5. Training Loss Function

By combining Eq. (6) and Eq. (8), our overall loss function for G-FRET can be written as:

$$\mathcal{L}_{GFRET} = \mathcal{L}_R + \lambda \mathcal{L}_P \tag{9}$$

where λ is the balancing hyperparameter that controls the trade-off between $\mathcal{L}_R$ and $\mathcal{L}_P$.

During testing, adaptation is performed online: upon receiving instances $\{x_i\}_{i=1}^{n_t}$ at time t, the model is updated with parameters from the previous instances. The model then generates the prediction $\{p_i = g(x_i)\}_{i=1}^{n_t}$ for the new instances and updates using Eq. (9) with a single step of gradient descent. Adaptation continues as long as test data is available.

4. Experiments and Analysis

In this section, we conduct extensive experiments to explore the following key questions: (1) Is Test-Time Adaptation (TTA) based on feature redundancy elimination truly effective? (Sec. 4.2) (2) Do the underlying mechanisms of S-FRET and G-FRET align with our theoretical assumptions? (Sec. 4.3) (3) Additionally, we perform ablation studies and evaluate the scalability of our method in more complex scenarios. Sec. 4.4)

4.1. Experimental Setup

We evaluate the adaptation performance on two main tasks: image domain adaptation and image corruption adaptation. Following previous studies, for domain adaptation, we use the PACS [21] dataset and the OfficeHome [47] dataset. For image corruption adaptation, we utilize the CIFAR10-C , CIFAR100-C and ImageNet-C [13] datasets. To implement label shifts, we adjust the CIFAR-100-C datasets to follow a long-tail distribution [7], denoted as CIFAR-100-C-LT. The comparison methods we employ include: BN [35], TENT [48] EATA [28], SAR [29], TSD [50], TIPI [27], and TEA [55]. Backbone networks include ResNet-18 and ResNet-50 [12]. To ensure fairness, we report mean and standard deviation of 5 runs with different random seeds and independently perform hyperparameter tuning for all methods to achieve the highest accuracy as their final results. Refer to Sec. 8 for more implement information. For further experimental results and analysis, please see Sec. 9.

4.2. Comparison with State-of-the-art Methods

4.2.1. Domain Generalization

Tab. 1 presents the accuracy comparison of S-FRET and G-FRET with other state-of-the-art TTA methods on the PACS and OfficeHome datasets based on ResNet-18 and ResNet-50 backbones.The table shows that S-FRET, through its simple yet effective optimization, attains competitive performance comparable to most existing TTA methods, while G-FRET achieves superior performance across both datasets and backbone types. Specifically, on the PACS dataset, G-FRET improves upon the baseline non-adaptive

Backbone	Method	PACS				Avg	OfficeHome				Avg
		A	C	P	S		A	C	P	R	
ResNet-18	Source [12]	78.37$_{\pm0.00}$	77.39$_{\pm0.00}$	95.03$_{\pm0.00}$	76.58$_{\pm0.00}$	81.84$_{\pm0.00}$	56.45$_{\pm0.00}$	48.02$_{\pm0.00}$	71.34$_{\pm0.00}$	72.23$_{\pm0.00}$	62.01$_{\pm0.00}$
	BN [35]	81.03$_{\pm0.09}$	80.67$_{\pm0.27}$	95.14$_{\pm0.15}$	73.83$_{\pm0.18}$	82.66$_{\pm0.08}$	55.66$_{\pm0.17}$	49.23$_{\pm0.32}$	70.73$_{\pm0.10}$	72.49$_{\pm0.19}$	62.03$_{\pm0.12}$
	SAR [29]	83.62$_{\pm0.42}$	81.47$_{\pm0.93}$	95.14$_{\pm0.15}$	80.44$_{\pm0.74}$	85.17$_{\pm0.26}$	57.30$_{\pm0.44}$	50.54$_{\pm0.26}$	70.71$_{\pm0.55}$	72.75$_{\pm0.27}$	62.82$_{\pm0.31}$
	EATA [28]	82.06$_{\pm0.85}$	81.11$_{\pm1.03}$	95.16$_{\pm0.29}$	73.39$_{\pm1.00}$	82.93$_{\pm0.46}$	56.42$_{\pm0.41}$	49.75$_{\pm0.41}$	71.50$_{\pm0.35}$	72.85$_{\pm0.41}$	62.63$_{\pm0.11}$
	TENT [48]	83.54$_{\pm1.78}$	82.26$_{\pm1.69}$	95.54$_{\pm0.31}$	81.05$_{\pm1.78}$	85.60$_{\pm0.75}$	57.25$_{\pm0.32}$	50.45$_{\pm0.26}$	72.18$_{\pm0.38}$	73.09$_{\pm0.34}$	63.24$_{\pm0.13}$
	TSD [50]	87.05$_{\pm0.47}$	86.94$_{\pm0.62}$	95.98$_{\pm0.25}$	82.56$_{\pm1.12}$	88.13$_{\pm0.44}$	**57.80**$_{\pm0.34}$	50.05$_{\pm0.69}$	71.45$_{\pm0.42}$	70.92$_{\pm0.46}$	62.55$_{\pm0.06}$
	TEA [55]	87.04$_{\pm0.54}$	86.54$_{\pm0.85}$	96.17$_{\pm0.36}$	82.17$_{\pm1.08}$	87.98$_{\pm0.48}$	57.07$_{\pm0.88}$	50.47$_{\pm0.18}$	71.84$_{\pm0.18}$	72.85$_{\pm0.10}$	63.06$_{\pm0.27}$
	TIPI [27]	84.79$_{\pm1.18}$	84.24$_{\pm1.01}$	95.86$_{\pm0.18}$	**84.05**$_{\pm0.75}$	87.23$_{\pm0.41}$	57.23$_{\pm0.34}$	50.42$_{\pm0.27}$	72.23$_{\pm0.24}$	73.28$_{\pm0.19}$	63.29$_{\pm0.05}$
	S-FRET	86.25$_{\pm0.30}$	86.66$_{\pm0.37}$	95.96$_{\pm0.25}$	75.90$_{\pm2.44}$	86.20$_{\pm0.66}$	56.26$_{\pm0.21}$	49.86$_{\pm0.38}$	71.65$_{\pm0.05}$	72.72$_{\pm0.14}$	62.62$_{\pm0.09}$
	G-FRET	**87.20**$_{\pm0.35}$	**87.19**$_{\pm0.24}$	**96.28**$_{\pm0.36}$	83.36$_{\pm1.43}$	**88.51**$_{\pm0.39}$	57.49$_{\pm0.34}$	**51.28**$_{\pm0.42}$	**73.04**$_{\pm0.29}$	**73.40**$_{\pm0.35}$	**63.81**$_{\pm0.11}$
ResNet-50	Source [12]	83.89$_{\pm0.00}$	81.02$_{\pm0.00}$	96.17$_{\pm0.00}$	78.04$_{\pm0.00}$	84.78$_{\pm0.00}$	64.85$_{\pm0.00}$	52.26$_{\pm0.00}$	75.04$_{\pm0.00}$	75.88$_{\pm0.00}$	67.01$_{\pm0.00}$
	BN [35]	85.19$_{\pm0.35}$	85.49$_{\pm0.30}$	96.60$_{\pm0.19}$	72.25$_{\pm0.33}$	84.88$_{\pm0.08}$	63.30$_{\pm0.20}$	53.02$_{\pm0.32}$	73.59$_{\pm0.23}$	75.10$_{\pm0.29}$	66.25$_{\pm0.05}$
	SAR [29]	85.24$_{\pm0.37}$	85.49$_{\pm0.30}$	96.60$_{\pm0.19}$	76.02$_{\pm0.84}$	85.84$_{\pm0.26}$	64.78$_{\pm0.17}$	56.30$_{\pm0.57}$	74.83$_{\pm0.27}$	76.18$_{\pm0.30}$	68.02$_{\pm0.19}$
	EATA [28]	85.14$_{\pm0.31}$	85.36$_{\pm0.20}$	96.54$_{\pm0.19}$	72.27$_{\pm0.11}$	84.83$_{\pm0.11}$	64.25$_{\pm0.41}$	54.09$_{\pm0.53}$	74.25$_{\pm0.36}$	75.72$_{\pm0.43}$	67.08$_{\pm0.22}$
	TENT [48]	87.07$_{\pm0.87}$	86.76$_{\pm0.52}$	96.92$_{\pm0.20}$	78.83$_{\pm1.97}$	87.40$_{\pm0.69}$	64.53$_{\pm0.21}$	55.15$_{\pm0.59}$	74.68$_{\pm0.38}$	76.19$_{\pm0.14}$	67.64$_{\pm0.19}$
	TSD [50]	90.83$_{\pm0.89}$	89.94$_{\pm0.27}$	97.56$_{\pm0.27}$	81.56$_{\pm1.52}$	89.97$_{\pm0.18}$	65.33$_{\pm0.30}$	56.99$_{\pm0.34}$	76.12$_{\pm0.36}$	76.52$_{\pm0.24}$	68.74$_{\pm0.14}$
	TEA [55]	88.51$_{\pm0.43}$	87.75$_{\pm0.51}$	97.17$_{\pm0.24}$	81.45$_{\pm1.02}$	88.72$_{\pm0.26}$	65.62$_{\pm0.45}$	57.55$_{\pm0.64}$	75.80$_{\pm0.39}$	76.85$_{\pm0.51}$	68.95$_{\pm0.25}$
	TIPI [27]	87.62$_{\pm0.73}$	86.97$_{\pm0.96}$	97.01$_{\pm0.11}$	79.66$_{\pm1.50}$	87.81$_{\pm0.56}$	64.92$_{\pm0.29}$	56.47$_{\pm0.37}$	75.31$_{\pm0.27}$	76.74$_{\pm0.37}$	68.36$_{\pm0.04}$
	S-FRET	89.90$_{\pm0.60}$	89.00$_{\pm0.48}$	97.46$_{\pm0.32}$	77.45$_{\pm0.91}$	88.45$_{\pm0.19}$	64.42$_{\pm0.20}$	55.06$_{\pm0.34}$	75.56$_{\pm0.24}$	76.41$_{\pm0.14}$	67.86$_{\pm0.13}$
	G-FRET	**90.99**$_{\pm0.87}$	**90.00**$_{\pm0.25}$	**97.59**$_{\pm0.29}$	**82.32**$_{\pm2.59}$	**90.23**$_{\pm0.53}$	**66.12**$_{\pm0.41}$	**57.63**$_{\pm0.39}$	**76.46**$_{\pm0.34}$	**77.19**$_{\pm0.23}$	**69.35**$_{\pm0.20}$

Table 1. Accuracy comparison of different TTA methods on PACS and OfficeHome datasets based on ResNet-18 and ResNet-50 backbones, including mean and standard deviation of 5 runs with different random seeds. The best results are highlighted in **boldface**, and the second ones are underlined.

source model by 6.67% and 5.45% with ResNet-18 and ResNet-50, respectively. For OfficeHome, the improvements are 1.80% and 2.34%, respectively. Compared with state-of-the-art TTA methods, G-FRET achieves the highest or second-highest accuracy overall, particularly when using the ResNet-50 as backbone, G-FRET consistently achieves the highest accuracy across all domains. In contrast, other methods fail to achieve consistently high accuracy across different domains and backbones. This is caused by G-FRET's ability to consider both feature discriminability and redundancy.

4.2.2. Image Corruption

Tab. 2 shows the accuracy comparisons of S-FRET and G-FRET and other state-of-the-art methods for image corruption on CIFAR-10-C , CIFAR-100-C, and ImageNet-C at damage level of 5. We designed two experimental settings: continuous adaptation and independent adaptation. For CIFAR-10/100-C, the model undergoes continuous adaptation, where all 15 corruption types are applied sequentially. For ImageNet-C, each corruption type is evaluated independently on the adapted model. The results demonstrate that S-FRET significantly outperforms the baseline non-adaptive source model and achieves average performance increases of 22.84% on CIFAR-10-C, 17.52% on CIFAR-100-C and 14.4% on ImageNet-C. It can be observed that G-FRET consistently outperforms S-FRET. This is because S-FRET only considers feature redundancy without incorporating label distribution information, whereas G-FRET accounts for both feature redundancy and discriminability. For continuous adaptation, compared to other methods that do not explicitly minimize feature redundancy, their performance is similar to S-FRET but inferior to G-FRET. This indicates that both feature redundancy reduction and traditional class discriminative information contribute to continuous TTA performance, and their combination further enhances adaptation. This finding is further validated in the subsequent ablation studies.

Method	CIFAR-10-C			CIFAR-100-C			ImageNet-C		
	1-7	8-15	1-15	1-7	8-15	1-15	1-7	8-15	1-15
Source [12]	38.46	61.59	50.80	23.59	37.49	31.01	7.74	20.79	14.70
BN [35]	70.47	76.43	73.65	45.70	50.57	48.30	17.84	36.12	27.59
TENT [48]	73.06	79.25	76.36	47.77	53.44	50.79	27.05	42.69	35.39
EATA [28]	70.60	76.42	73.70	47.64	53.40	50.71	**31.23**	**46.15**	**39.19**
SAR [29]	70.61	76.50	73.75	46.66	51.21	49.09	30.37	45.70	38.55
TIPI [27]	**73.76**	80.21	77.21	47.50	52.06	49.93	27.78	42.69	35.73
TEA [55]	71.70	77.47	74.78	46.07	50.64	48.51	22.85	40.72	32.38
TSD [50]	72.53	77.96	75.43	45.87	51.03	48.62	20.93	38.15	30.11
S-FRET	71.60	77.28	74.63	46.31	50.46	48.53	19.59	37.43	29.10
G-FRET	**73.76**	**80.32**	**77.26**	**48.23**	**53.55**	**51.06**	28.60	43.96	36.79

Table 2. Accuracy comparison of different TTA methods on CIFAR-10/100-C and ImageNet-C datasets at damage level of 5, with 15 types of damage applied two experimental settings: continuous adaptation and independent adaptation.

4.2.3. Efficiency Comparison

In addition to accuracy, we also evaluate the runtime efficiency of different methods to assess the computational performance of S-FRET and G-FRET. As shown in Tab. 3, "Training" indicates whether the method involves retraining. ERM represents the source model without adaptation,

while the BN method directly updates the batch normalization (BN) parameters, eliminating the need for retraining. Consequently, BN is the most computationally efficient method. However, as reported in Tabs. 1 and 2, BN consistently exhibits the lowest accuracy. Among the traning methods, S-FRET achieves the lowest runtime across different backbones, whereas G-FRET operates at an average runtime compared to other baselines. These results indicate that S-FRET, as a simple yet effective approach, provides a competitive accuracy-efficiency trade-off. Meanwhile, G-FRET, despite its moderate computational cost, achieves the highest accuracy, demonstrating its effectiveness in balancing efficiency and adaptation performance.

Cost Time (s)										
Backbone	ERM	BN	TENT	EATA	SAR	TSD	TIPI	TEA	S-FRET	G-FRET
Traning	×	×	✓	✓	✓	✓	✓	✓	✓	✓
ResNet-18	39	36	48	56	74	114	162	658	**46**	118
ResNet-50	64	66	113	109	185	153	264	1376	**102**	193
VIT-B/16	141	162	210	220	345	295	281	3181	**185**	310
AVG	81	88	124	128	201	187	236	1738	**111**	207

Table 3. Cost time comparison of TTA methods on ImageNet-C (Gaussian Noise) across multiple backbone networks

4.3. Analysis of Underlying Mechanisms

4.3.1. Relation between Feature Redundancy Elimination and Generalizability Enhancement

The first mechanism to be validated is whether there exists a genuine relationship between feature redundancy and generalizability enhancement. We track the evolution of normalized redundancy scores (NRS), loss, and accuracy across increasing adaptation steps. As shown in Fig. 3, S-FRET achieves a consistent reduction in feature redundancy as adaptation progresses, accompanied by stable accuracy improvement, demonstrating the detrimental effect of redundancy on generalization and the efficacy of redundancy elimination. For G-FRET, as the number of adaptation steps increases, there is also a consistent reduction in the redundancy of the extracted embedded features, accompanied by a significant decrease in loss and a notable improvement in accuracy. In summary, both S-FRET and G-FRET has been demonstrated to be highly effective in minimizing redundancy, and redundancy elimination is strongly associated with enhancement of model generalizability.

4.3.2. Label Shift

Is S-FRET truly affected by label shift? Tab. 4 presents the performance of S-FRET and G-FRET under test-time label shifts with long-tailed distributions. Here, the imbalance factor denotes the ratio between the most and least frequent class samples—higher values indicate more skewed class distributions. As shown in Tab. 4, S-FRET achieves competitive performance on CIFAR-100-C under balanced

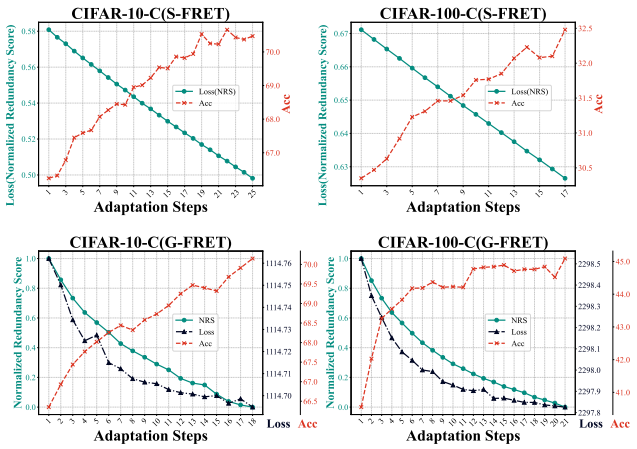

Figure 3. The relationship of the reduction of redundancy and the enhancement of generalizability attained by S-FRET and G-FRET on CIFAR-10-C and CIFAR-100-C datasets. NRS: Normalized Redundancy Scores.

CIFAR-100-C-LT										
Imbalance Factor	ERM	BN	SAR	EATA	TENT	TSD	TIPI	TEA	S-FRET	G-FRET
1	31.01	48.30	49.09	50.71	50.79	48.62	48.51	49.93	48.53	**51.06**
10	30.39	47.14	47.69	47.86	50.12	47.74	47.50	49.54	47.47	**50.23**
100	30.13	46.07	48.21	46.08	49.80	46.95	47.13	49.51	46.62	**50.27**
AVG	30.51	47.17	48.33	48.21	50.24	47.77	47.71	49.66	47.54	**50.52**

Table 4. Performance comparison on CIFAR-100-C-LT with different imbalance factors based on ResNet-18.

class distributions. However, its accuracy degrades significantly as the imbalance factor increases, with 1.91% drops on CIFAR-100-C, aligning with the limitations of conventional TTA methods. In contrast, G-FRET delivers more robust performance across all imbalance factors. This highlights G-FRET's unique capability to address label shift in real-world scenarios through contrastive learning.

4.3.3. Discriminability Analysis by tSNE

Does G-FRET truly improve discriminability compared to S-FRET? Fig. 4 shows the t-SNE [45] visualization of embedded features before and after adaptation by S-FRET and G-FRET. It is evident that before adaptation, data points from different classes are intermixed without clear separation. After adaptation by S-FRET, although class separation increases, the overlapping regions between classes still lack distinct boundaries. In contrast, G-FRET achieves more distinct cluster separation and sharper decision boundaries, demonstrating its superior capability in learning discriminative features under distribution shifts.

4.4. Ablation and Extension Study

4.4.1. Effects of Components in G-FRET

Tab. 5 presents the impact of the four components of G-FRET on model performance. (1) Compared to the source baseline, each individual component contributes positively

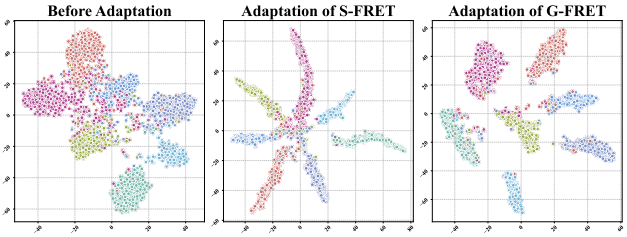

Figure 4. Discriminability visualization of embedded feature before and after adaptation by S-FRET and G-FRET respectively.

OfficeHome								
Components			A	C	P	R	AVG	↑
Source			56.45	48.02	71.34	72.23	62.01	0.00
Individual	$\mathcal{L}_R$	A	55.83	49.67	70.83	72.89	62.31	0.30
		R	56.98	50.42	72.33	72.73	63.12	1.11
	$\mathcal{L}_P$	A	56.73	50.77	72.13	72.99	63.16	1.15
		R	55.83	49.30	70.62	72.51	62.07	0.06
Ablation	w/o $\mathcal{L}_R$	A	57.72	51.18	72.99	73.08	63.74	1.73
		R	56.70	51.16	72.07	73.19	63.28	1.27
	w/o $\mathcal{L}_P$	A	57.11	50.52	72.40	72.94	63.24	1.23
		R	57.77	51.40	72.94	72.96	63.77	1.76
Attention	$\mathcal{L}_R(A)$+$\mathcal{L}_P(A)$		56.70	50.97	72.36	73.12	63.29	1.28
Redundant	$\mathcal{L}_R(R)$+$\mathcal{L}_P(R)$		57.03	50.49	72.27	72.94	63.18	1.17
All	All		57.49	51.28	73.04	74.40	**63.81**	**1.80**

Table 5. Effects of components in G-FRET, test on the OfficeHome dataset with ResNet-18 backbone. A: Attention part, R: Redundancy Part.

to the model's performance, with respective gains of 0.30%, 1.11%, 1.15%, and 0.06%. Notably, the redundancy component in the representation layer, $\mathcal{L}_R(R)$, and the attention component in the prediction layer, $\mathcal{L}_P(A)$, show the most significant impact, with $\mathcal{L}_R(R)$ achieving a 1.15% improvement. This highlights the importance of redundancy reduction for TTA. (2) The ablation study further confirms the significance of each component, indicating that their removal negatively impacts model performance. (3) Either the redundant or attention components can individually improves model performance, with respective gains of 1.28% and 1.17%. When the two components are jointly considered, they yield an even greater improvement. (4) Overall, the experimental results further validate the necessity of considering feature redundancy during the TTA process.

4.4.2. Parameter Sensitivity

Our method G-FRET involves one hyperparameter: the trade-off parameter in Eq. (9), λ. As shown in Fig. 5, G-FRET outperforms the source model across a wide range of values for λ. We also investigate the impact of the learning rate (lr) on the experimental results. The best performance is achieved with a learning rate of around 1×10^{-4}; higher learning rates tend to destabilize the training process and reduce the effectiveness of model, which is also observed in

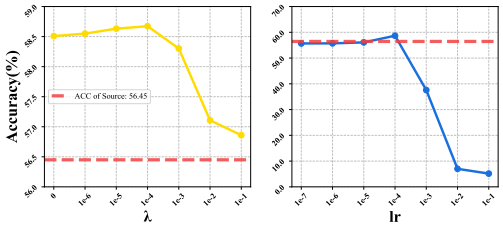

Figure 5. Parameter sensitivity analysis G-FRET on the OfficeHome dataset with ResNet-18 backbone in domain Art.

Method	VLCS[44]	DomainNet[33]	ImageNet-C[13]
ResNet-18 [12]	73.67	39.13	14.70
+S-FRET	73.90	39.26	29.10
+G-FRET	**75.73**	**40.22**	**36.79**
ResNet-50 [12]	74.90	43.58	18.15
+S-FRET	75.48	43.69	34.65
+G-FRET	**76.42**	**44.22**	**42.84**
VIT-B/16 [6]	76.44	49.98	39.83
+S-FRET	77.18	51.22	60.36
+G-FRET	**78.56**	**51.50**	**62.50**

Table 6. Scalability on complex/large dataset and different backbones.

other TTA methods [27–29, 48, 50, 55].

4.4.3. Scalability on complex/large dataset and different backbones.

We validated our method on more complex and larger datasets, as well as on a VIT [6] backbone, to ensure that our approach can robustly improve performance and is not dependent on any specific network architecture. Tab. 6 demonstrates that the proposed methods generally enhances baseline performance across different backbones. Even on large and complex datasets such as ImageNet-C[13], our method demonstrates significant improvements across different backbones, with S-FRET achieving performance gains of 14.4%, 16.5%, 20.53% and G-FRET attaining 22.09%, 24.69%, 22.67%, respectively.

5. Conclusion

In this work, we propose a novel approach for test-time adaptation (TTA) — Feature Redundancy Elimination for TTA (FRET) — which focuses on reducing feature redundancy during testing to address distribution shifts. This is the first attempt to leverage feature redundancy for TTA. We introduce two methods: S-FRET, which directly minimizes the feature redundancy score, and G-FRET, which optimizes both redundancy elimination and class discriminability by decomposing feature relations into attention and redundancy components. Experiments across various tasks and datasets show the effectiveness of S-FRET and G-FRET, demonstrating the value of feature redundancy elim-

ination in TTA.

References

[1] Ivan Anishchenko, Samuel J Pellock, Tamuka M Chidyausiku, Theresa A Ramelot, Sergey Ovchinnikov, Jingzhou Hao, Khushboo Bafna, Christoffer Norn, Alex Kang, Asim K Bera, et al. De novo protein design by deep network hallucination. *Nature*, 600(7889):547–552, 2021.

[2] Gavin Brown, Adam Pocock, Ming-Jie Zhao, and Mikel Luján. Conditional likelihood maximisation: a unifying framework for information theoretic feature selection. *The journal of machine learning research*, 13(1):27–66, 2012.

[3] Kaidi Cao, Colin Wei, Adrien Gaidon, Nikos Arechiga, and Tengyu Ma. Learning imbalanced datasets with label distribution-aware margin loss. In *Proc. the Advances in Neural Information Processing Systems (NeurIPS)*, pages 1567–1578, 2019.

[4] Xue-wen Chen and Jong Cheol Jeong. Enhanced recursive feature elimination. In *Sixth international conference on machine learning and applications (ICMLA 2007)*, pages 429–435. IEEE, 2007.

[5] Ian Connick Covert, Wei Qiu, Mingyu Lu, Na Yoon Kim, Nathan J White, and Su-In Lee. Learning to maximize mutual information for dynamic feature selection. In *International Conference on Machine Learning*, pages 6424–6447. PMLR, 2023.

[6] Alexey Dosovitskiy. An image is worth 16x16 words: Transformers for image recognition at scale. *arXiv preprint arXiv:2010.11929*, 2020.

[7] C. Du, Y. Wang, S. Song, and G. Huang. Probabilistic contrastive learning for long-tailed visual recognition. *IEEE Transactions on Pattern Analysis and Machine Intelligence*, 46(9):5890–5904, 2024.

[8] Tongtong Fang, Nan Lu, Gang Niu, and Masashi Sugiyama. Rethinking importance weighting for deep learning under distribution shift. *Advances in neural information processing systems*, 33:11996–12007, 2020.

[9] Ronald A Fisher. The use of multiple measurements in taxonomic problems. *Annals of eugenics*, 7(2):179–188, 1936.

[10] Taesik Gong, Yewon Kim, Taeckyung Lee, Sorn Chottananurak, and Sung-Ju Lee. Sotta: Robust test-time adaptation on noisy data streams. *Advances in Neural Information Processing Systems*, 36, 2024.

[11] Jie Gui, Zhenan Sun, Shuiwang Ji, Dacheng Tao, and Tieniu Tan. Feature selection based on structured sparsity: A comprehensive study. *IEEE transactions on neural networks and learning systems*, 28(7):1490–1507, 2016.

[12] Kaiming He, Xiangyu Zhang, Shaoqing Ren, and Jian Sun. Deep residual learning for image recognition. In *Proceedings of the IEEE conference on computer vision and pattern recognition*, pages 770–778, 2016.

[13] Dan Hendrycks and Thomas Dietterich. Benchmarking neural network robustness to common corruptions and perturbations. *arXiv preprint arXiv:1903.12261*, 2019.

[14] Chenping Hou, Ruidong Fan, Ling-Li Zeng, and Dewen Hu. Adaptive feature selection with augmented attributes. *IEEE Transactions on Pattern Analysis and Machine Intelligence*, 45(8):9306–9324, 2023.

[15] John Jumper, Richard Evans, Alexander Pritzel, Tim Green, Michael Figurnov, Olaf Ronneberger, Kathryn Tunyasuvunakool, Russ Bates, Augustin Žídek, Anna Potapenko, et al. Highly accurate protein structure prediction with alphafold. *nature*, 596(7873):583–589, 2021.

[16] Bingyi Kang, Saining Xie, Marcus Rohrbach, Zhicheng Yan, Albert Gordo, Jiashi Feng, and Yannis Kalantidis. Decoupling representation and classifier for long-tailed recognition. In *Proc. the International Conference on Learning Representations (ICLR)*, 2019.

[17] Thomas N Kipf and Max Welling. Semi-supervised classification with graph convolutional networks. *arXiv preprint arXiv:1609.02907*, 2016.

[18] Yann LeCun, Yoshua Bengio, and Geoffrey Hinton. Deep learning. *nature*, 521(7553):436–444, 2015.

[19] Jonghyun Lee, Dahuin Jung, Saehyung Lee, Junsung Park, Juhyeon Shin, Uiwon Hwang, and Sungroh Yoon. Entropy is not enough for test-time adaptation: From the perspective of disentangled factors. In *The Twelfth International Conference on Learning Representations*, 2024.

[20] Taeckyung Lee, Sorn Chottananurak, Taesik Gong, and Sung-Ju Lee. Aetta: Label-free accuracy estimation for test-time adaptation. In *Proceedings of the IEEE/CVF Conference on Computer Vision and Pattern Recognition*, pages 28643–28652, 2024.

[21] Da Li, Yongxin Yang, Yi-Zhe Song, and Timothy M Hospedales. Deeper, broader and artier domain generalization. In *Proceedings of the IEEE international conference on computer vision*, pages 5542–5550, 2017.

[22] Jundong Li, Kewei Cheng, Suhang Wang, Fred Morstatter, Robert P Trevino, Jiliang Tang, and Huan Liu. Feature selection: A data perspective. *ACM computing surveys (CSUR)*, 50(6):1–45, 2017.

[23] Junnan Li, Pan Zhou, Caiming Xiong, and Steven C.H. Hoi. Prototypical contrastive learning of unsupervised representations. In *ICLR*, 2021.

[24] Jian Liang, Ran He, and Tieniu Tan. A comprehensive survey on test-time adaptation under distribution shifts. *International Journal of Computer Vision*, pages 1–34, 2024.

[25] Duy MH Nguyen, Hoang Nguyen, Nghiem Diep, Tan Ngoc Pham, Tri Cao, Binh Nguyen, Paul Swoboda, Nhat Ho, Shadi Albarqouni, Pengtao Xie, et al. Lvm-med: Learning large-scale self-supervised vision models for medical imaging via second-order graph matching. *Advances in Neural Information Processing Systems*, 36, 2024.

[26] Wamidh K Mutlag, Shaker K Ali, Zahoor M Aydam, and Bahaa H Taher. Feature extraction methods: a review. In *Journal of Physics: Conference Series*, page 012028. IOP Publishing, 2020.

[27] A Tuan Nguyen, Thanh Nguyen-Tang, Ser-Nam Lim, and Philip HS Torr. Tipi: Test time adaptation with transformation invariance. In *Proceedings of the IEEE/CVF Conference on Computer Vision and Pattern Recognition*, pages 24162–24171, 2023.

[28] Shuaicheng Niu, Jiaxiang Wu, Yifan Zhang, Yaofo Chen, Shijian Zheng, Peilin Zhao, and Mingkui Tan. Efficient

test-time model adaptation without forgetting. In *International conference on machine learning*, pages 16888–16905. PMLR, 2022.

[29] Shuaicheng Niu, Jiaxiang Wu, Yifan Zhang, Zhiquan Wen, Yaofo Chen, Peilin Zhao, and Mingkui Tan. Towards stable test-time adaptation in dynamic wild world. In *Internetional Conference on Learning Representations*, 2023.

[30] Aaron van den Oord, Yazhe Li, and Oriol Vinyals. Representation learning with contrastive predictive coding. *arXiv preprint arXiv:1807.03748*, 2018.

[31] Sung Kyu Park, Seunghan Yang, Jaegul Choo, and Sungrack Yun. Label shift adapter for test-time adaptation under covariate and label shifts. *2023 IEEE/CVF International Conference on Computer Vision (ICCV)*, pages 16375–16385, 2023.

[32] Adam Paszke, Sam Gross, Francisco Massa, Adam Lerer, James Bradbury, Gregory Chanan, Trevor Killeen, Zeming Lin, Natalia Gimelshein, Luca Antiga, et al. Pytorch: An imperative style, high-performance deep learning library. *Advances in neural information processing systems*, 32, 2019.

[33] Xingchao Peng, Qinxun Bai, Xide Xia, Zijun Huang, Kate Saenko, and Bo Wang. Moment matching for multi-source domain adaptation. In *Proceedings of the IEEE/CVF international conference on computer vision*, pages 1406–1415, 2019.

[34] Sharan Ramjee and Aly El Gamal. Efficient wrapper feature selection using autoencoder and model based elimination. *arXiv preprint arXiv:1905.11592*, 2019.

[35] Steffen Schneider, Evgenia Rusak, Luisa Eck, Oliver Bringmann, Wieland Brendel, and Matthias Bethge. Improving robustness against common corruptions by covariate shift adaptation. *Advances in neural information processing systems*, 33:11539–11551, 2020.

[36] Claude Elwood Shannon. A mathematical theory of communication. *The Bell system technical journal*, 27(3):379–423, 1948.

[37] David Silver, Aja Huang, Chris J Maddison, Arthur Guez, Laurent Sifre, George Van Den Driessche, Julian Schrittwieser, Ioannis Antonoglou, Veda Panneershelvam, Marc Lanctot, et al. Mastering the game of go with deep neural networks and tree search. *nature*, 529(7587):484–489, 2016.

[38] Samarth Sinha, Peter Gehler, Francesco Locatello, and Bernt Schiele. Test: Test-time self-training under distribution shift. In *Proceedings of the IEEE/CVF Winter Conference on Applications of Computer Vision (WACV)*, pages 2759–2769, 2023.

[39] Yongyi Su, Xun Xu, and Kui Jia. Towards real-world test-time adaptation: Tri-net self-training with balanced normalization. In *Proceedings of the AAAI Conference on Artificial Intelligence*, pages 15126–15135, 2024.

[40] Yongyi Su, Xun Xu, Tianrui Li, and Kui Jia. Revisiting realistic test-time training: Sequential inference and adaptation by anchored clustering regularized self-training. *IEEE Transactions on Pattern Analysis and Machine Intelligence*, 2024.

[41] Yue Tan, Chen Chen, Weiming Zhuang, Xin Dong, Lingjuan Lyu, and Guodong Long. Is heterogeneity notorious? taming heterogeneity to handle test-time shift in federated learning. *Advances in Neural Information Processing Systems*, 36, 2024.

[42] Dipti Theng and Kishor K Bhoyar. Feature selection techniques for machine learning: a survey of more than two decades of research. *Knowledge and Information Systems*, 66(3):1575–1637, 2024.

[43] Robert Tibshirani. Regression shrinkage and selection via the lasso. *Journal of the Royal Statistical Society Series B: Statistical Methodology*, 58(1):267–288, 1996.

[44] Antonio Torralba and Alexei A Efros. Unbiased look at dataset bias. In *CVPR 2011*, pages 1521–1528. IEEE, 2011.

[45] Laurens van der Maaten and Geoffrey E. Hinton. Visualizing data using t-sne. *Journal of Machine Learning Research*, 9: 2579–2605, 2008.

[46] B Venkatesh and J Anuradha. A review of feature selection and its methods. *Cybernetics and information technologies*, 19(1):3–26, 2019.

[47] Hemanth Venkateswara, Jose Eusebio, Shayok Chakraborty, and Sethuraman Panchanathan. Deep hashing network for unsupervised domain adaptation. In *Proceedings of the IEEE conference on computer vision and pattern recognition*, pages 5018–5027, 2017.

[48] Dequan Wang, Evan Shelhamer, Shaoteng Liu, Bruno Olshausen, and Trevor Darrell. Tent: Fully test-time adaptation by entropy minimization. *arXiv preprint arXiv:2006.10726*, 2020.

[49] Mei Wang and Weihong Deng. Deep visual domain adaptation: A survey. *Neurocomputing*, 312:135–153, 2018.

[50] Shuai Wang, Daoan Zhang, Zipei Yan, Jianguo Zhang, and Rui Li. Feature alignment and uniformity for test time adaptation. In *Proceedings of the IEEE/CVF Conference on Computer Vision and Pattern Recognition*, pages 20050–20060, 2023.

[51] Svante Wold, Kim Esbensen, and Paul Geladi. Principal component analysis. *Chemometrics and intelligent laboratory systems*, 2(1-3):37–52, 1987.

[52] Yanan Wu, Zhixiang Chi, Yang Wang, Konstantinos N Plataniotis, and Songhe Feng. Test-time domain adaptation by learning domain-aware batch normalization. In *Proceedings of the AAAI Conference on Artificial Intelligence*, pages 15961–15969, 2024.

[53] Kaichao You, Mingsheng Long, Zhangjie Cao, Jianmin Wang, and Michael I Jordan. Universal domain adaptation. In *Proceedings of the IEEE/CVF conference on computer vision and pattern recognition*, pages 2720–2729, 2019.

[54] Longhui Yuan, Binhui Xie, and Shuang Li. Robust test-time adaptation in dynamic scenarios. In *Proceedings of the IEEE/CVF Conference on Computer Vision and Pattern Recognition*, pages 15922–15932, 2023.

[55] Yige Yuan, Bingbing Xu, Liang Hou, Fei Sun, Huawei Shen, and Xueqi Cheng. Tea: Test-time energy adaptation. In *Proceedings of the IEEE/CVF Conference on Computer Vision and Pattern Recognition*, pages 23901–23911, 2024.

[56] Han Yue, Jundong Li, and Hongfu Liu. Second-order unsupervised feature selection via knowledge contrastive distillation. *IEEE Transactions on Pattern Analysis and Machine Intelligence*, 2023.

[57] Longbin Zeng, Jiayi Han, Liang Du, and Weiyang Ding. Rethinking precision of pseudo label: Test-time adaptation via complementary learning. *Pattern Recognition Letters*, 177: 96–102, 2024.

[58] Kaiyang Zhou, Ziwei Liu, Yu Qiao, Tao Xiang, and Chen Change Loy. Domain generalization: A survey. *IEEE Transactions on Pattern Analysis and Machine Intelligence*, 45(4):4396–4415, 2022.

FRET: Feature Redundancy Elimination for Test Time Adaptation

Supplementary Material

6. Extended Related Work

6.1. Test-Time Adaptation

In realistic scenarios, test data often undergoes natural variations or corruptions, resulting in data distribution shifts between the training and test phases. Recently, various Test-Time Adaptation (TTA) approaches have been proposed to adapt pre-trained models during testing [41, 54]. For batch normalization calibration methods, BN [35] replaces the activation statistics estimated from the training set with those of the test set. For pseudo-labeling methods, TSD [50] filters out unreliable features or predictions with high entropy, as lower entropy typically indicates higher accuracy, and it further filters unreliable samples using a consistency filter. For consistency training methods, TIPI [27] identifies input transformations that can simulate domain shifts and uses regularizers, based on derived bounds, to ensure the network remains invariant to such transformations. For clustering-based training methods, TENT [48] minimizes the prediction entropy of the model on the target data. EATA [28] selects reliable samples to minimize entropy loss during test-time adaptation and uses a Fisher regularizer to stabilize key parameters. The importance of these parameters is estimated from test samples with pseudo labels. SAR [29] removes noisy samples with large gradients and encourages model weights to reach a flat minimum, enhancing robustness against remaining noise. Recently, TEA [55], a state-of-the-art TTA approach, introduces an innovative energy-based perspective to mitigate the effects of distribution changes and has shown advantages over current leading approaches.

6.2. Feature Redundancy Elimination

Feature redundancy is a key concern in both feature extraction and feature selection [26, 42]. Feature extraction methods aim to reduce redundancy by transforming the original feature space into a new low-dimensional feature space while retaining as much relevant information as possible. Two typical feature extraction methods are unsupervised method Principal Component Analysis (PCA) [51] and supervised method Linear Discriminant Analysis (LDA) [9]. The former one performs a linear transformation to create a new feature space where the features are uncorrelated, while the latter one reduces redundancy by identifying feature spaces that best separate different classes by maximizing the between-class dispersion while minimizing within-class dispersion.

Unlike feature extraction, feature selection aims to identify the most representative and non-redundant subset of features from the original feature set [46]. Feature selection methods generally include three strategies: 1) Filter methods [2, 5] use statistical measures (e.g., mutual information, Fisher score) to evaluate feature relevance and redundancy. Features with high relevance are deemed more informative for target variables, while redundant features are removed to enhance feature independence. 2) Wrapper methods [34] assess feature subsets by training models and evaluating their performance. A common wrapper method is Recursive Feature Elimination (RFE) [4], which iteratively removes features and evaluates model performance to identify the optimal subset. 3) Embedded methods [11, 14] integrate feature selection within the model training process, such as Lasso regression [43], which penalizes redundant features during training to optimize model parameters and select the most relevant features. Recently, a novel feature selection approach called SOFT [56] has been proposed, which combines second-order covariance matrices with first-order data matrices by knowledge contrastive distillation for unsupervised feature selection.

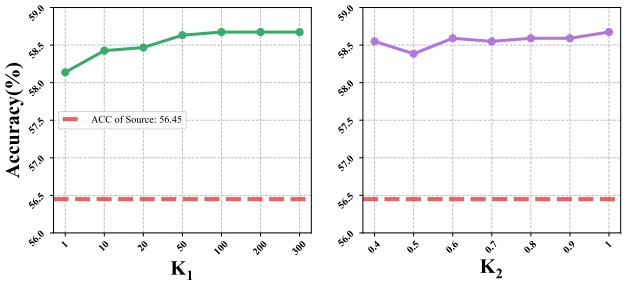

Figure 6. Sensitivity analysis of two G-FRET filtering parameters using ResNet-18 on OfficeHome's Art domain.

7. Some Filter Tricks

Following the previous works [28, 48, 50], to reduce the influence of wrong and noisy results from model g, which may create some incorrect computations, we use Shannon entropy [36] to filter unreliable instances. Specifically, for each class, we only take the representations with the top-K_1 lowest output entropy H_i into computing class centers:

$$H_i = -\sum \sigma(p_i) \log \sigma(p_i) \tag{10}$$

Furthermore, we use the similarity between representation and class centers to generate soft pseudo labels $\hat{y}_i$ for the ith instance, which can be formulated as:

$$\hat{y}_i = \sigma\left([\text{sim}(R_{A_i}, c_1), \text{sim}(R_{A_i}, c_2), \ldots, \text{sim}(R_{A_i}, c_C)]\right) \tag{11}$$

Based on this, we only consider the predictions with the top-K_2 percent lowest output entropy in a data batch while keeping label consistency between pseudo labels and their predictions, i.e., $\text{argmax}(p_i) = \text{argmax}(\hat{y}_i)$, when computing L_R and L_P. We evaluate the effectiveness of these filter tricks on G-FRET. As shown in Fig. 6, G-FRET exhibits insensitivity to K_1, and K_2.

8. Experimental details

8.1. Datasets

We evaluate the performance of the S-FRET and G-FRET on two main tasks: domain generalization and image corruption generalization. Following previous studies, for domain generalization, we use the PACS [21] dataset, consisting of images from seven categories (e.g., objects, animals) across four domains (art paintings, cartoons, photos, and sketches), and the OfficeHome [47] dataset, which includes 65 categories (e.g., office items, home objects) from four domains (art, clipart, product, and real-world images). For image corruption generalization, we utilize the CIFAR10-C , CIFAR100-C and ImageNet-C [13] datasets, which contain 15 types of corruption at five severity levels. To be consistent with prior research [20], all experiments are conducted at the highest severity level (level 5). To implement label shifts, we adjust the CIFAR-100-C datasets to follow a long-tail distribution [7], denoted as CIFAR-100-C-LT.

8.2. Comparison Methods

The comparison methods we employ include the non-adaptive source model and four baseline methods which are commonly used in several studies: BN [35], TENT [48], EATA [28], and SAR [29]. Additionally, we adopt three recently proposed state-of-the-art methods: TSD [50], TIPI [27], and TEA [55].

8.3. Models and Implementation

For domain generalization tasks, we use ResNet-18/50 [12] with batch normalization as the backbone network. These networks are pretrained on data from three domains and then tested on the remaining domain.

For image corruption, we use ResNet-18 as the backbone network. We train it on the clean versions of the CIFAR-10 and CIFAR-100 datasets, and for ImageNet-C, we leverage pre-trained model from TorchVision. When it comes to CIFAR-10/100-C, we apply all 15 corruption types sequentially to assess continuous adaptation capabilities. For ImageNet-C, we apply each of the 15 corruption types independently to the adapted model.

To ensure fairness, we report mean and standard deviation of 5 runs with different random seeds (0, 1, 2, 3, 4). In addition, we set the batch size as 128 during testing and independently perform hyperparameter tuning for each method to achieve the highest possible accuracy as the final result. All implementations are carried out using PyTorch [32] and executed on a single NVIDIA 4090 GPU for all experiments.

8.4. Complex/Large Dataset

VLCS [44] contains four domains: Caltech101, LabelMe, SUN09, and VOC2007, with a total of 10,729 images across 5 classes. The label distribution across the domains in VLCS exhibits substantial variation , which might be a contributing factor to the poor performance of most Test-Time Adaptation methods on this dataset [50].

DomainNet [33] is a large-scale dataset used in transfer learning, consisting of six domains: Clipart, Infograph, Painting, Quickdraw, Real, and Sketch. It consists of a total of 586,575 images, with each domain containing 345 classes.

ImageNet-C [13] is significantly larger compared to the CIFAR10-C and CIFAR100-C. CIFAR10-C and CIFAR100-C consist of 50,000 training images and 10,000 test images each, divided into 10 and 100 classes respectively. In contrast, ImageNet-C contains 1,281,167 training images and 50,000 test images, categorized into 1,000 classes. Specifically, ImageNet-C encompasses 15 types of corruption with five levels of severity. In our experiments, we employed the highest corruption level (level 5). For the pre-trained model on ImageNet-C, we utilize the model provided by TorchVision.

8.5. Experiment Setting Details

For hyper-parameter selection in Domain Generalization task (Sec. 4.2.1), we first identify the optimal parameter set based on the highest accuracy achieved on the default domain (art paintings in PACS and art in OfficeHome). These parameters are then applied to other domains to assess their performance. Specifically, we conduct a search for the learning rate within the range {1e-7, 5e-7, 1e-6, 5e-6, 1e-5, 5e-5, 1e-4, 5e-4, 1e-3, 5e-3, 1e-2, 5e-2}. For methods that include an entropy filter component (e.g., TSD, G-FRET), we explore the entropy filter hyperparameter in the set {1, 5, 10, 15, 20, 50, 100, 200, 300}. For the G-FRET, we perform hyperparameter tuning for λ within the range {1e-6, 1e-5, 1e-4, 1e-3, 1e-2, 1e-1, 1, 10, 100} and K_2 within the values {0.5, 0.6, 0.7, 0.8, 0.9, 1}.

For the Image Corruption task (Sec. 4.2.2), each Test-Time Adaptation (TTA) method continuously adapts to 15 types of image corruptions in the specified order for CIFAR-10/100-C: [Gaussian Noise, Shot Noise, Impulse Noise, Defocus Blur, Glass Blur, Motion Blur, Zoom Blur, Snow,

Frost, Fog, Brightness, Contrast, Elastic Transformation, Pixelate, JPEG Compression]. However, for ImageNet-C, we adopt a strategy of independently adapting to each of the 15 corruption types separately. The hyperparameter ranges remain consistent with those utilized in Domain Generalization. The best performance results obtained for each method are selected as the final experimental outcomes.

9. Additional Experimental Results

9.1. Detailed Results Across Five Random Seeds

To ensure the fairness of our evaluation, we conduct experiments using five different random seeds (0, 1, 2, 3, and 4). The detailed results corresponding to each random seed are presented in Tabs. 7 to 11, which highlights the robustness and consistency of our proposed methods S-FRET and G-FRET.

9.2. Detailed Results for Image Corruption

In this section, we provide a complete listing of comparisons between S-FRET, G-FRET, and other state-of-the-art methods for Image Corruption (Sec. 4.2.2) on CIFAR-10/100-C and ImageNet-C datasets at damage level of 5, as shown in Tabs. 12 to 14.

9.3. Detailed Results for Scalability Experiment

In the Scalability experiment (Sec. 4.4.3), we validate our methods using larger and more complex datasets including VLCS, DomainNet, and ImageNet-C, as well as on the ViT backbone, to demonstrate that our approach can robustly improve performance across diverse datasets and different backbones.

For VLCS and DomainNet, we employ hyperparameter selection within the same range as the Domain Generalization task. However, unlike the Domain Generalization task, we independently selected hyperparameters for each domain rather than applying the parameters from the default domain to others.

For ImageNet-C, we adapt the TTA method to each corruption type individually. We select hyperparameters optimized for the default corruption type (Gaussian Noise), and applied these parameters to other corruption types. The detailed results are presented in Tab. 15, Tab. 16 , and Tab. 17 .

Backbone	Method	PACS				Avg	OfficeHome				Avg
		A	C	P	S		A	C	P	R	
ResNet-18	Source [12]	78.37	77.39	95.03	76.58	81.84	56.45	48.02	71.34	72.23	62.01
	BN [35]	80.91	80.80	95.09	73.84	82.66	55.62	49.32	70.60	72.66	62.05
	SAR [29]	83.30	82.17	95.09	79.69	85.06	57.15	50.31	70.24	72.34	62.51
	EATA [28]	82.71	81.53	94.91	74.19	83.34	56.41	49.62	71.66	72.27	62.49
	TENT [48]	82.76	82.68	95.33	78.19	84.74	56.94	50.65	71.86	72.92	63.09
	TSD [50]	**86.96**	86.73	96.41	81.22	87.83	58.06	49.81	71.37	70.67	62.47
	TEA [55]	86.47	85.79	95.69	80.81	87.19	**58.63**	50.56	71.95	72.92	63.52
	TIPI [27]	85.50	84.90	96.05	**83.13**	87.39	57.03	50.61	72.07	**73.28**	63.25
	S-FRET	86.28	86.69	96.35	74.22	85.88	56.20	50.08	71.57	72.64	62.62
	G-FRET	86.82	**87.03**	**96.65**	81.29	**87.95**	57.73	**51.36**	**73.10**	72.99	**63.79**
ResNet-50	Source [12]	83.89	81.02	96.17	78.04	84.78	64.85	52.26	75.04	75.88	67.01
	BN [35]	85.50	85.62	96.77	72.05	84.99	63.54	52.71	73.89	75.05	66.30
	SAR [29]	85.55	85.62	96.77	75.24	85.79	64.77	55.92	75.24	75.81	67.94
	EATA [28]	84.67	85.20	96.35	72.36	84.64	63.91	54.04	74.72	75.51	67.05
	TENT [48]	88.09	87.33	97.19	79.69	88.07	64.61	54.80	75.06	76.20	67.67
	TSD [50]	90.43	89.89	**97.84**	81.80	89.99	65.27	56.77	76.19	76.41	68.66
	TEA [55]	88.09	87.88	97.49	81.39	88.71	66.25	**57.50**	75.20	76.68	68.91
	TIPI [27]	88.18	87.93	97.13	78.80	88.01	64.73	56.24	75.47	77.00	68.36
	S-FRET	89.99	89.51	**97.84**	76.30	88.41	64.15	54.50	75.74	76.25	67.66
	G-FRET	**90.72**	**90.15**	**97.84**	**82.29**	**90.25**	**66.42**	57.11	**76.21**	**77.35**	**69.27**

Table 7. At random seed 0, the accuracy comparison of different TTA methods on PACS and OfficeHome datasets based on ResNet-18 and ResNet-50 backbones. The best results are highlighted in **boldface**, and the second ones are underlined.

Backbone	Method	PACS				Avg	OfficeHome				Avg
		A	C	P	S		A	C	P	R	
ResNet-18	Source [12]	78.37	77.39	95.03	76.58	81.84	56.45	48.02	71.34	72.23	62.01
	BN [35]	81.10	80.59	95.33	73.84	82.71	55.83	48.80	70.78	72.21	61.90
	SAR [29]	84.33	80.03	95.33	79.59	84.82	56.90	50.22	70.06	72.89	62.52
	EATA [28]	82.96	82.47	95.45	73.00	83.47	57.03	50.13	71.03	72.96	62.79
	TENT [48]	84.91	81.19	95.57	82.82	86.12	57.77	50.22	72.56	72.62	63.29
	TSD [50]	86.62	86.39	95.87	81.50	87.59	57.52	49.26	72.18	71.20	62.54
	TEA [55]	**87.79**	86.60	95.99	82.21	88.15	56.78	**50.70**	72.02	72.85	63.09
	TIPI [27]	85.11	83.23	95.87	**85.03**	87.31	**57.81**	50.19	72.56	72.96	63.38
	S-FRET	85.84	86.69	95.93	72.84	85.33	56.53	49.51	71.71	72.53	62.57
	G-FRET	87.26	**86.99**	**96.59**	82.74	**88.39**	57.23	50.61	**73.51**	**73.17**	**63.63**
ResNet-50	Source [12]	83.89	81.02	96.17	78.04	84.78	64.85	52.26	75.04	75.88	67.01
	BN [35]	85.01	85.88	96.65	71.88	84.85	63.00	53.54	73.60	74.96	66.27
	SAR [29]	85.01	85.88	96.65	75.92	85.86	65.06	56.31	74.50	76.45	68.08
	EATA [28]	85.35	85.41	96.71	72.23	84.92	64.81	53.88	73.80	75.60	67.02
	TENT [48]	86.23	86.95	97.01	79.77	87.49	64.81	55.58	74.75	76.38	67.88
	TSD [50]	**89.75**	89.63	**97.49**	83.76	90.16	65.72	57.14	76.39	76.18	68.86
	TEA [55]	89.16	88.05	96.89	82.54	89.16	65.22	57.69	75.67	**77.37**	68.99
	TIPI [27]	87.16	86.99	97.07	80.99	88.05	65.39	56.11	75.69	76.27	68.36
	S-FRET	89.36	89.46	97.37	78.57	88.69	64.61	55.28	75.60	76.50	68.00
	G-FRET	**89.75**	**89.97**	**97.49**	**85.52**	**90.68**	**66.17**	**57.87**	**76.93**	76.80	**69.44**

Table 8. At random seed 1, the accuracy comparison of different TTA methods on PACS and OfficeHome datasets based on ResNet-18 and ResNet-50 backbones. The best results are highlighted in **boldface**, and the second ones are underlined.

Backbone	Method	PACS				Avg	OfficeHome				Avg
		A	C	P	S		A	C	P	R	
ResNet-18	Source [12]	78.37	77.39	95.03	76.58	81.84	56.45	48.02	71.34	72.23	62.01
	BN [35]	81.05	80.42	94.97	73.73	82.54	55.71	49.10	70.85	72.55	62.05
	SAR [29]	83.69	82.08	94.97	81.01	85.44	57.11	50.70	71.03	72.76	62.90
	EATA [28]	80.91	81.06	94.97	72.77	82.43	56.49	49.10	71.95	73.22	62.69
	TENT [48]	81.20	83.70	95.51	81.42	85.46	57.19	50.42	71.80	73.08	63.12
	TSD [50]	87.06	87.12	95.93	83.07	88.29	**57.48**	51.11	71.23	70.32	62.54
	TEA [55]	87.09	**87.97**	**96.47**	81.50	88.26	56.53	50.42	71.91	72.96	62.96
	TIPI [27]	82.86	84.04	95.93	**84.58**	86.85	57.19	50.49	72.00	73.45	63.28
	S-FRET	86.28	86.35	95.69	78.34	86.66	56.04	49.46	71.64	72.89	62.51
	G-FRET	**87.45**	87.07	96.35	83.66	**88.63**	57.23	**51.59**	**72.85**	**73.84**	**63.88**
ResNet-50	Source [12]	83.89	81.02	96.17	78.04	84.78	64.85	52.26	75.04	75.88	67.01
	BN [35]	84.72	85.20	96.59	72.72	84.80	63.33	53.08	73.64	74.82	66.22
	SAR [29]	84.72	85.20	96.59	75.18	85.42	64.73	56.93	74.86	76.15	68.17
	EATA [28]	85.45	85.11	**96.47**	72.38	84.85	63.86	54.73	74.00	75.60	67.05
	TENT [48]	87.06	85.92	96.65	75.34	86.24	64.32	55.60	74.09	76.02	67.51
	TSD [50]	**91.85**	**89.76**	97.49	79.92	**89.75**	64.89	57.46	75.76	76.54	68.66
	TEA [55]	88.57	88.27	97.07	**80.48**	88.60	65.93	57.00	75.96	76.25	68.78
	TIPI [27]	**87.45**	85.41	96.89	77.53	86.82	64.85	56.98	75.02	76.41	68.31
	S-FRET	90.77	88.69	97.31	77.07	88.46	64.44	55.40	75.26	76.29	67.85
	G-FRET	**91.85**	89.59	**97.54**	78.42	89.35	**66.05**	**57.73**	**76.17**	**77.25**	**69.30**

Table 9. At random seed 2, the accuracy comparison of different TTA methods on PACS and OfficeHome datasets based on ResNet-18 and ResNet-50 backbones. The best results are highlighted in **boldface**, and the second ones are underlined.

Backbone	Method	PACS				Avg	OfficeHome				Avg
		A	C	P	S		A	C	P	R	
ResNet-18	Source [12]	78.37	77.39	95.03	76.58	81.84	56.45	48.02	71.34	72.23	62.01
	BN [35]	80.96	80.46	95.03	74.12	82.64	55.75	49.67	70.76	72.64	62.20
	SAR [29]	83.40	81.02	95.03	81.01	85.11	57.27	50.68	70.80	73.08	62.96
	EATA [28]	82.23	80.84	94.97	72.31	82.59	56.32	49.97	71.53	72.57	62.60
	TENT [48]	83.15	79.91	95.27	82.08	85.10	57.03	50.77	72.09	73.40	63.32
	TSD [50]	86.77	86.52	95.93	83.61	88.21	**57.85**	49.85	71.37	71.52	62.65
	TEA [55]	**87.26**	86.26	**96.59**	83.61	88.43	56.70	50.42	71.75	72.69	62.89
	TIPI [27]	84.57	83.40	95.57	83.69	86.81	56.94	50.72	72.11	73.26	63.26
	S-FRET	86.18	86.35	96.05	75.82	86.10	56.12	50.36	71.68	72.80	62.74
	G-FRET	86.87	**87.33**	95.87	**84.07**	**88.53**	57.31	**51.64**	**72.76**	**73.65**	**63.84**
ResNet-50	Source [12]	83.89	81.02	96.17	78.04	84.78	64.85	52.26	75.04	75.88	67.01
	BN [35]	85.16	85.20	96.71	72.18	84.81	63.41	52.88	73.26	75.58	66.28
	SAR [29]	85.40	85.20	96.71	76.86	86.04	64.73	56.77	74.75	76.50	68.19
	EATA [28]	85.21	85.49	96.41	72.10	84.80	64.15	53.36	74.41	75.42	66.83
	TENT [48]	86.18	86.90	96.95	79.97	87.50	64.32	55.51	74.93	76.27	67.76
	TSD [50]	90.48	**90.32**	97.78	81.98	90.14	65.31	56.59	75.74	76.75	68.60
	TEA [55]	88.13	86.95	97.07	82.41	88.64	65.27	**58.56**	76.23	**77.39**	**69.36**
	TIPI [27]	86.77	87.54	97.07	81.04	88.10	64.65	56.72	75.20	77.09	68.42
	S-FRET	89.31	88.95	97.72	78.16	88.54	64.61	55.10	75.38	76.59	67.92
	G-FRET	**90.82**	90.23	**97.90**	**83.46**	**90.60**	**65.47**	57.34	**76.28**	77.32	69.10

Table 10. At random seed 3, the accuracy comparison of different TTA methods on PACS and OfficeHome datasets based on ResNet-18 and ResNet-50 backbones. The best results are highlighted in **boldface**, and the second ones are underlined.

Backbone	Method	PACS				Avg	OfficeHome				Avg
		A	C	P	S		A	C	P	R	
ResNet-18	Source [12]	78.37	77.39	95.03	76.58	81.84	56.45	48.02	71.34	72.23	62.01
	BN [35]	81.10	81.06	95.27	73.63	82.77	55.38	49.28	70.65	72.39	61.92
	SAR [29]	83.40	82.04	95.27	80.91	85.40	58.06	50.79	71.39	72.66	63.23
	EATA [28]	81.49	79.65	95.51	74.68	82.83	55.87	49.92	71.34	73.22	62.59
	TENT [48]	85.69	83.83	96.05	80.73	86.58	57.31	50.17	72.61	**73.42**	63.38
	TSD [50]	**87.84**	**87.93**	95.75	83.41	88.73	**58.10**	50.22	71.10	70.87	62.57
	TEA [55]	86.57	86.05	**96.13**	82.72	87.87	56.70	50.22	71.57	72.85	62.83
	TIPI [27]	85.89	85.62	95.87	83.84	87.80	57.19	50.10	72.40	**73.42**	63.28
	S-FRET	86.67	87.24	95.81	78.29	87.00	56.41	49.90	71.66	72.71	62.67
	G-FRET	87.60	87.54	95.93	**85.06**	**89.03**	57.97	**51.20**	**72.99**	73.38	**63.89**
ResNet-50	Source [12]	83.89	81.02	96.17	78.04	84.78	64.85	52.26	75.04	75.88	67.01
	BN [35]	85.55	85.58	96.29	72.41	84.96	63.21	52.90	73.55	75.07	66.18
	SAR [29]	85.55	85.58	96.29	76.89	86.08	64.61	55.56	74.79	75.97	67.73
	EATA [28]	85.01	85.58	96.77	72.26	84.90	64.52	54.46	74.30	76.47	67.44
	TENT [48]	87.79	86.69	96.83	79.41	87.68	64.61	54.27	74.59	76.11	67.39
	TSD [50]	91.65	**90.10**	97.19	80.33	89.82	65.47	57.00	76.53	76.73	68.93
	TEA [55]	88.57	87.59	**97.37**	80.40	88.48	65.43	57.02	75.92	76.54	68.73
	TIPI [27]	88.53	86.99	96.89	79.94	88.09	64.98	56.29	75.20	76.91	68.34
	S-FRET	90.09	88.40	97.07	77.14	88.17	64.28	55.03	75.83	76.45	67.90
	G-FRET	**91.80**	90.06	97.19	**81.93**	**90.24**	**66.50**	**58.08**	**76.71**	**77.23**	**69.63**

Table 11. At random seed 4, the accuracy comparison of different TTA methods on PACS and OfficeHome datasets based on ResNet-18 and ResNet-50 backbones. The best results are highlighted in **boldface**, and the second ones are underlined.

Method	$t \longrightarrow$															Avg
	Gau.	Sho.	Imp.	Def.	Gla.	Mot.	Zoo.	Sno.	Fro.	Fog	Bri.	Con.	Ela.	Pix.	Jpe.	
Source [12]	27.43	33.56	21.57	43.64	40.48	51.26	51.29	68.18	54.52	66.65	87.50	27.59	67.06	48.86	72.37	50.80
BN [35]	66.30	68.18	57.13	82.50	57.44	79.73	81.98	74.83	74.12	78.91	86.96	82.02	70.23	73.43	70.94	73.65
TENT [48]	67.26	71.46	61.21	84.07	61.37	81.66	84.36	78.18	77.55	80.14	88.44	81.41	73.54	78.53	76.19	76.36
EATA [28]	66.39	68.50	57.32	82.52	57.42	79.94	82.09	74.80	74.14	78.90	86.98	81.93	70.10	73.62	70.88	73.70
SAR [29]	66.46	68.24	57.47	82.52	57.83	79.76	81.98	74.83	74.29	78.92	86.96	82.36	70.26	73.43	70.94	73.75
TIPI [27]	67.57	**72.14**	**62.88**	84.19	**63.55**	81.63	84.44	**79.06**	**79.07**	79.61	88.68	81.92	**75.33**	**79.92**	**78.11**	77.21
TEA [55]	66.71	69.24	59.46	82.78	59.98	80.87	82.88	76.40	75.60	79.82	86.72	81.48	71.89	74.91	72.91	74.78
TSD [50]	66.97	70.31	60.63	83.24	61.10	81.52	83.97	77.15	76.75	80.08	86.76	80.42	72.66	76.43	73.42	75.43
S-FRET	66.52	69.45	59.40	82.78	59.43	80.64	82.98	76.05	75.73	79.59	86.92	80.68	71.56	75.11	72.61	74.63
G-FRET	**67.79**	71.83	62.81	**84.31**	62.63	**82.07**	**84.89**	78.91	79.00	**81.01**	**88.87**	**82.69**	74.86	79.47	77.74	**77.26**

Table 12. Accuracy comparisons of different TTA methods on CIFAR-10-C dataset at damage level of 5, with 15 types of damage applied sequentially to a continuously adapted model. The best results are highlighted in **boldface**, and the second ones are underlined.

Method	$t \longrightarrow$															Avg
	Gau.	Sho.	Imp.	Def.	Gla.	Mot.	Zoo.	Sno.	Fro.	Fog	Bri.	Con.	Ela.	Pix.	Jpe.	
Source [12]	10.46	12.49	3.36	34.44	23.63	38.10	42.67	39.25	33.01	32.84	55.78	11.55	46.48	34.88	46.15	31.01
BN [35]	39.84	39.51	29.88	56.43	41.08	54.34	58.82	48.52	49.36	46.60	61.82	48.78	49.92	54.17	45.39	48.30
TENT [48]	40.61	41.94	32.09	57.84	44.35	56.57	60.96	51.51	52.03	49.23	**63.94**	49.62	53.53	**57.60**	50.03	50.79
EATA [28]	40.59	41.82	32.58	**57.97**	43.43	56.76	60.33	50.79	51.90	48.71	63.83	49.88	53.96	**57.60**	50.50	50.71
SAR [29]	40.09	40.67	31.52	57.01	42.16	55.63	59.54	50.53	50.31	47.73	62.50	43.27	51.03	55.49	48.80	49.09
TIPI [27]	40.62	42.29	32.67	57.06	**44.84**	55.45	59.58	**52.19**	52.15	46.33	61.91	43.60	52.20	57.39	50.67	49.93
TEA [55]	40.13	39.90	30.82	56.28	41.48	54.73	59.16	48.79	49.31	46.26	61.41	48.48	50.22	54.03	46.63	48.51
TSD [50]	39.84	39.65	30.14	56.63	41.17	54.65	59.03	48.71	49.71	47.25	61.95	48.84	50.65	54.78	46.36	48.62
S-FRET	39.84	39.94	31.10	56.66	42.01	55.19	59.46	48.66	49.21	47.21	61.52	46.80	50.66	53.88	45.75	48.53
G-FRET	**41.08**	**43.23**	**33.69**	57.49	44.07	**56.87**	**61.16**	51.24	**52.18**	**49.25**	63.12	**50.04**	**54.09**	57.42	**51.02**	**51.06**

Table 13. Accuracy comparisons of different TTA methods on CIFAR-100-C dataset at damage level of 5, with 15 types of damage applied sequentially to a continuously adapted model. The best results are highlighted in **boldface**, and the second ones are underlined.

Method	ImageNet-C															Avg
	Gau.	Sho.	Imp.	Def.	Gla.	Mot.	Zoo.	Sno.	Fro.	Fog	Bri.	Con.	Ela.	Pix.	Jpe.	
Source [12]	1.54	2.27	1.48	11.44	8.68	11.12	17.62	10.64	16.21	14.02	51.52	3.44	16.49	23.35	30.67	14.70
BN [35]	13.65	14.84	14.17	11.95	13.04	23.34	33.89	29.18	28.42	40.80	58.11	12.09	38.92	44.35	37.08	27.59
TENT [48]	23.45	25.71	24.08	18.79	20.90	33.54	42.85	39.64	32.95	50.36	60.13	10.68	48.81	51.96	46.98	35.39
EATA [28]	**28.24**	**30.16**	**28.88**	**25.30**	**25.74**	**36.61**	43.71	**41.80**	36.42	50.87	59.12	**31.75**	49.10	52.33	47.82	**39.19**
SAR [29]	28.04	29.59	27.88	23.66	23.90	36.16	43.40	40.94	**36.71**	**51.01**	60.18	27.38	48.95	**52.47**	**47.98**	38.55
TIPI [27]	24.45	26.52	24.75	20.37	22.25	33.65	42.46	39.31	33.47	49.93	59.44	12.53	48.41	51.51	46.92	35.73
TEA [55]	18.82	20.50	19.00	16.27	17.68	28.51	39.17	35.19	32.26	46.92	59.16	15.42	44.39	48.81	43.64	32.38
TSD [50]	15.60	16.99	16.13	15.59	15.41	28.69	38.07	32.92	30.01	45.90	58.69	7.62	41.06	47.47	41.52	30.11
S-FRET	15.04	16.40	15.57	13.77	14.67	25.65	36.00	31.08	29.08	43.13	58.64	12.33	40.37	45.76	39.07	29.10
G-FRET	24.85	27.47	25.49	20.82	22.71	35.10	**43.76**	40.66	36.68	50.80	**60.3**	14.20	**49.28**	52.24	47.52	36.79

Table 14. Accuracy comparisons of different TTA methods on ImageNet-C dataset at damage level of 5, with 15 types of damage applied independently to the adapted model based on ResNet-18. The best results are highlighted in **boldface**, and the second ones are underlined.

Method	VLCS				Avg
	C	L	S	V	
ResNet-18	94.49	60.96	67.73	71.50	73.67
+S-FRET	96.11	59.71	67.28	72.51	73.90
+G-FRET	**96.68**	**64.42**	**67.82**	**73.99**	**75.73**
ResNet-50	95.55	**60.77**	71.12	72.16	74.90
+S-FRET	96.05	57.89	69.86	**78.10**	75.48
+G-FRET	**96.96**	58.51	**72.27**	77.93	**76.42**
ViT-B/16	97.81	64.38	69.71	73.84	76.44
+S-FRET	97.81	67.32	69.59	73.99	77.18
+G-FRET	**98.52**	**68.00**	**73.49**	**74.23**	**78.56**

Table 15. Accuracy on the VLCS dataset with different backbones: ResNet-18/50 and ViT-B/16.

Method	DomainNet						Avg
	C	I	P	Q	R	S	
ResNet-18	57.30	**16.86**	45.03	12.69	56.89	46.00	39.13
+S-FRET	57.69	12.58	44.55	15.18	**57.71**	47.86	39.26
+G-FRET	**58.97**	14.10	**46.16**	**15.22**	57.42	**49.48**	**40.22**
ResNet-50	63.68	**20.93**	50.35	12.95	62.16	51.42	43.58
+S-FRET	63.95	15.72	50.00	**15.23**	**63.51**	53.09	43.59
+G-FRET	**64.85**	17.61	**51.19**	14.71	63.33	**53.61**	**44.22**
ViT-B/16	71.91	25.56	55.95	18.36	70.66	57.45	49.98
+S-FRET	72.30	**27.17**	**59.45**	17.25	71.48	59.65	51.22
+G-FRET	**72.63**	26.04	58.28	**18.92**	**72.61**	**60.50**	**51.50**

Table 16. Accuracy on the DomainNet dataset with different backbones: ResNet-18/50 and ViT-B/16.

Method	ImageNet-C															Avg
	Gau.	Sho.	Imp.	Def.	Gla.	Mot.	Zoo.	Sno.	Fro.	Fog	Bri.	Con.	Ela.	Pix.	Jpe.	
ResNet-18	1.54	2.27	1.48	11.44	8.68	11.12	17.62	10.64	16.21	14.02	51.52	3.44	16.49	23.35	30.67	14.70
+S-FRET	15.04	16.40	15.57	13.77	14.67	25.65	36.00	31.08	29.08	43.13	58.64	12.33	40.37	45.76	39.07	29.10
+G-FRET	**24.85**	**27.47**	**25.49**	**20.82**	**22.71**	**35.10**	**43.76**	**40.66**	**36.68**	**50.80**	**60.30**	**14.20**	**49.28**	**52.24**	**47.52**	**36.79**
ResNet-50	3.00	3.70	2.64	17.91	9.74	14.71	22.45	16.60	23.06	24.01	59.12	5.38	16.51	20.87	32.63	18.15
+S-FRET	19.26	18.81	19.91	18.66	18.16	29.96	43.32	38.29	34.02	51.74	66.52	16.69	47.22	52.51	44.60	34.65
+G-FRET	**29.22**	**29.13**	**29.83**	**25.99**	**26.68**	**44.10**	**50.83**	**49.15**	**43.40**	**58.43**	**67.35**	**17.88**	**57.12**	**59.68**	**53.76**	**42.84**
ViT-B/16	35.09	32.16	35.88	31.42	25.31	39.45	31.55	24.47	30.13	54.74	64.48	48.98	34.20	53.17	56.45	39.83
+S-FRET	51.62	53.02	53.54	49.54	50.21	56.68	**59.19**	**61.93**	**61.22**	70.65	72.85	65.43	66.11	67.87	65.61	60.36
+G-FRET	**57.56**	**56.80**	**58.02**	**56.86**	**57.42**	**62.11**	58.98	41.25	59.39	**72.69**	**77.31**	**70.33**	**66.61**	**71.93**	**70.25**	**62.50**

Table 17. Accuracy on the ImageNet-C dataset with different backbones: ResNet-18/50 and ViT-B/16.